Inorganic Chemistry
Article
pubs.acs.org/IC

Electrochemical Synthesis of a Lithium-Rich Rock-Salt-Type Oxide $Li_5W_2O_7$ with Reversible Deintercalation Properties

Valerie Pralong,* Gopal Venkatesh, Sylvie Malo, Vincent Caignaert, Radu Baies, and Bernard Raveau

Laboratoire CRISMAT, CNRS ENSICAEN, 6 bd Maréchal Juin, 14050 Caen, France

ABSTRACT: Starting from the ribbon structure $Li_2W_2O_7$, the lithium-rich phase $Li_5W_2O_7$ with an ordered rock-salt-type structure has been synthesized, through a topotactic irreversible reaction, using both electrochemistry and soft chemistry. In contrast to $Li_2W_2O_7$, the lithium-rich oxide $Li_5W_2O_7$ shows reversible deintercalation properties of two lithium molecules per formula unit: a stable reversible capacity of 110 mAh/g at 1.70 V is maintained after 10 cycles. The exploration of the lithium mobility in this system shows that $Li_2W_2O_7$ is a cationic conductor with $\sigma = 4.10^{-4}$ S/cm at 400 °C and $E_a = 0.5$ eV.

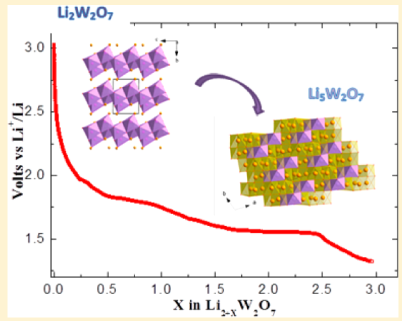

■ INTRODUCTION

The association of lithium to a transition metal (M) in oxides is a very efficient route for generating new materials with intercalation properties susceptible to use as electrodes in lithium-ion batteries.[1−4] Such behavior is a consequence of three criteria: (i) the high mobility of Li^+, (ii) the ability of the transition element to adopt a mixed valence varying with the intercalated lithium content, (iii) the rather small size difference between the Li^+ and M^{n+} cations, compared to Na^+, allowing lithium-rich close-packed structures to be formed. Thus, the electrochemical intercalation of lithium in transition-metal oxides of various elements—cobalt, manganese, nickel, vanadium, titanium, and molybdenum—with different structures has allowed lithium-rich rock-salt-type oxides to be synthesized (see for review ref 5). Remarkably, these rock-salt oxides show reversible lithium intercalation/deintercalation properties.

An understanding of the lithium intercalation/deintercalation process in these close-packed transition-metal oxides is an important issue, which has so far not really been elucidated, especially for lithium-rich compounds. In this respect, the Li−W−O system is very attractive because of the ability of tungsten to adopt various oxidation states and coordinations, with values of the redox potentials of 2.4 and 1.6 V for the couples W^{6+}/W^{5+} and W^{5+}/W^{4+}, respectively. Curiously, except for WO_3,[6−8] no lithium tungstate W^{VI} was investigated either for ionic conductivity or from the electrochemical lithium intercalation viewpoint, in spite of the existence of several lithium tungstates, such as $Li_2W_2O_7$,[9,10] Li_2WO_4,[11] and Li_4WO_5.[12] On the basis of these considerations, we have investigated the ionic conductivity and lithium intercalation in the tungstate $Li_2W_2O_7$. Herein, we show that $Li_2W_2O_7$ with a ribbon structure can intercalate up to three lithium ions per formula, leading to the rock-salt-type oxide $Li_5W_2O_7$, through an irreversible electrochemical topotactic reaction. Moreover, we have demonstrated that, in contrast, $Li_5W_2O_7$ can deintercalate/intercalate reversibly two Li^+ cations per formula unit at an average potential of 1.70 V with a reversible capacity of 110 mAh/g.

■ EXPERIMENTAL SECTION

Synthesis of the Precursor $Li_2W_2O_7$. The parent phase $Li_2W_2O_7$ was prepared via a regular solid-state method starting from Li_2CO_3 and WO_3 in a stoichiometric ratio at 500 °C for 24 h with intermediate grindings. The average size of the agglomerated particles was 10 μm in size. The powder X-ray diffraction (PXRD) pattern showed the formation of a pure $Li_2W_2O_7$ phase, which was refined by the Rietveld method. The refined lattice parameters are in good agreement with the previous reports.[7] This phase could be described as a ribbon-type structure built up of distorted WO_6 octahedra and LiO_4 tetrahedra. The edge-sharing WO_6 octahedra form $[W_2O_7]_\infty$ ribbons running along the *c* axis.

Electrochemical Synthesis and Characterization. The electrochemistry characterization of $Li_2W_2O_7$ was performed in Swagelok cells. The negative electrode was metallic lithium (Aldrich, 99,9%), LP30 from Merck [1 M $LiPF_6$ in an ethylene carbonate/dimethyl carbonate 1:1 (w/w) Selectipur], and used as the electrolyte, and the positive electrode was constituted of approximately 10 mg of a mixture of the active material with 30% carbon (acetylene black). The electrochemical cells were cycled at constant current between 1.3 and 3.0 V at different galvanostatic rates on a VMP II potentiostat/galvanostat (Biologic SA, Claix, France) at room temperature. Potentiostatic intermittent titration technique (PITT)[13] measurements were conducted using a potential step of 10 mV limited by a minimum current equivalent to a C/50 galvanostatic rate. Impedance measurements were carried out with a Solartron 1260 in the frequency range of 0.1 Hz to 1 MHz. Pellets were prepared by cold pressing of the powder sample. Platinum electrodes were deposited by vacuum evaporation. The impedance measurements were carried out at steady-state temperatures from room temperature to 500 °C under air.

Structural and Chemical Characterization. The compounds were characterized by PXRD using a Bruker D8 diffractometer with a capillary sample geometry and a Philips X'Pert diffractometer with

Received: October 8, 2013
Published: December 20, 2013

Bragg−Brentano geometry (Cu K$\alpha_{1,2}$ radiation). Note that, because of their instability in air, the PXRD patterns of the reduced phases $Li_{5-x}W_2O_7$ were registered under vacuum using a chamber attached to the Philips PXRD instrument. The electron diffraction (ED) studies were carried out on a JEOL 200CX electron microscope fitted with an eucentric goniometer (±60°) equipped with an energy-dispersive spectroscopy analyzer at room temperature. For the transmission electron microscopy study, the samples were crushed in *n*-butanol and deposited on a holey carbon membrane supported by a copper grid. The ED patterns were calculated with the *JEMS* v3.3708U2009 software. A ZEISS SUPRA 55 scanning electron microscope was used for morphology studies. The lithium content was determined by atomic absorption spectroscopy with a Varian Spectra AA-20 instrument. Thermogravimetric analysis (TGA) was performed in a N_2 atmosphere at a heating rate of 3 °C/min with a TG92 Setaram microbalance. The TGA study (not shown) revealed that this phase is stable up to 600 °C.

■ RESULTS AND DISCUSSION

Electrochemical and Chemical Intercalation of Lithium into $Li_2W_2O_7$: Synthesis of $Li_5W_2O_7$. The electrochemical intercalation of lithium into $Li_2W_2O_7$ was performed at *C*/100 rate, discharging the cell down to 1.3 V. The galvanostatic discharge curve and the corresponding derivative curve (Figure 1) show two plateaus: the first one for the insertion of one lithium at 1.70 V and the second one at 1.55 V with the insertion of two lithium molecules.

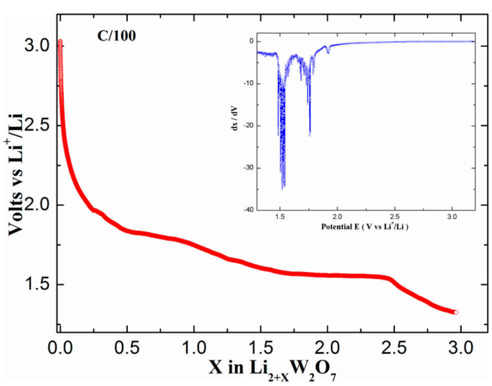

Figure 1. Voltage versus composition curve for the first discharge for $Li_2W_2O_7$ at *C*/100 rate to 2.0 V. Inset: corresponding derivative curve d*V*/d*t* versus Li^+/Li.

Such well-defined plateaus suggest the occurrence of biphasic processes with possibly generation of a new structure for the fully reduced phase with a composition of $Li_5W_2O_7$. To check this point, chemical reduction was performed in an argon-filled glovebox in order to avoid the activity loss of *n*-butyllithium (nBu-Li) and for safety reasons. Starting from 200 mg of $Li_2W_2O_7$ in a 10 mL solution of anhydrous hexane, 2.5 M nBu-Li in hexane was slowly added in excess (5 times) to the solution with a single-use 10 mL syringe. The resulting solution was stirred at room temperature for 5 days (equilibrium, 2.0 V vs NHE) at room temperature. In these conditions, the atomic absorption analysis indicates that insertion reaches three additional lithium molecules per formula unit, leading to a composition of $Li_5W_2O_7$ for the fully reduced sample. In Figure 2 are reported the ex situ PXRD patterns of the two limit compounds, before and after complete reduction. The PXRD pattern taken after insertion of three lithium molecules for $Li_5W_2O_7$ (Figure 2b) is very different from that of the parent phase $Li_2W_2O_7$ (Figure 2a), showing that at first sight the

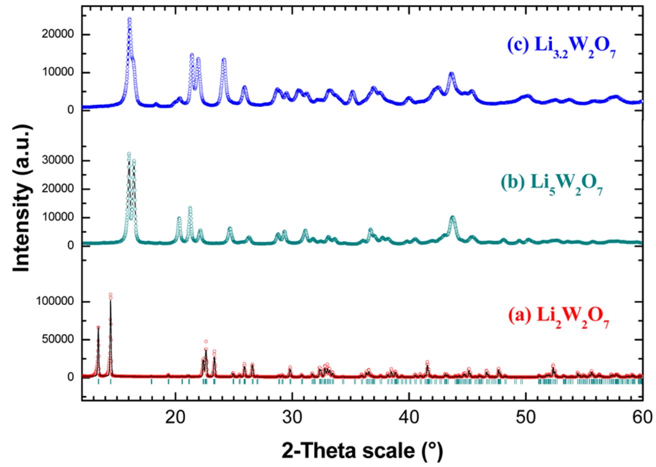

Figure 2. PXRD patterns of (a) pristine $Li_2W_2O_7$ [pattern matching profile (χ^2 < 15); the small bars indicate the angular positions of the allowed Bragg reflections], (b) reduced phase $Li_5W_2O_7$, and (c) oxidized phase $Li_{3.2}W_2O_7$.

relationships between the two structures are not straightforward. Thus, a detailed structural characterization was carried out.

Structural Study of $Li_5W_2O_7$. Bearing in mind that the electrochemical intercalation produces samples that contain amorphous carbon and that their corresponding phases are less well crystallized, the structural study was performed on the end member $Li_5W_2O_7$ prepared by nBu-Li reduction. The PXRD pattern registered with an X'Pert Philips diffractometer with Cu Kα radiation was indexed, using the first 20 reflections with the autoindexing software *DICVOL4*.[14] This program gave a unique triclinic solution with high figures of merit, $M(20)$ = 10.3 and $F(20)$ = 16.5. This solution was confirmed with the *TREOR*[15] program. The cell parameters of $Li_5W_2O_7$ (Table 1) are significantly different from those of $Li_2W_2O_7$, as expected from their PXRD patterns (Figure 2), confirming that the relationships between the two structures are not obvious.

Both oxides are triclinic, but only the *c* parameters and the β and γ angles are similar in the two structures. This triclinic cell is further supported by the ED patterns registered along [010] (Figure 3a) and [0−11] (Figure 3b).

In order to determine the positions of the heavier atoms, tungsten and oxygen, the PXRD pattern of this phase was then

Table 1. Crystallographic Data for $Li_xW_2O_7$, for x = 2 [18] and 5

	$Li_2W_2O_7$ [ref 9]	$Li_5W_2O_7$ chemical reduction
Space group	$P\bar{1}$	$P\bar{1}$
a (Å)	8.283(3)	9.2511(3)
b (Å)	7.050(1)	6.0443(2)
c (Å)	5.037(1)	5.0199(4)
α (deg)	85.40(2)	72.072(4)
β (deg)	102.13(3)	100.691(4)
γ (deg)	110.29(1)	108.321(2)
cell volume (Å^3)	269.72	252.30(2)
calcd density (g/cm^3)		6.771
χ^2		12.2
R_B (%)		12.5
R_{wp} (%)		9.76
average valency for W	+6	+4.5

dx.doi.org/10.1021/ic402543e | *Inorg. Chem.* 2014, 53, 522−527

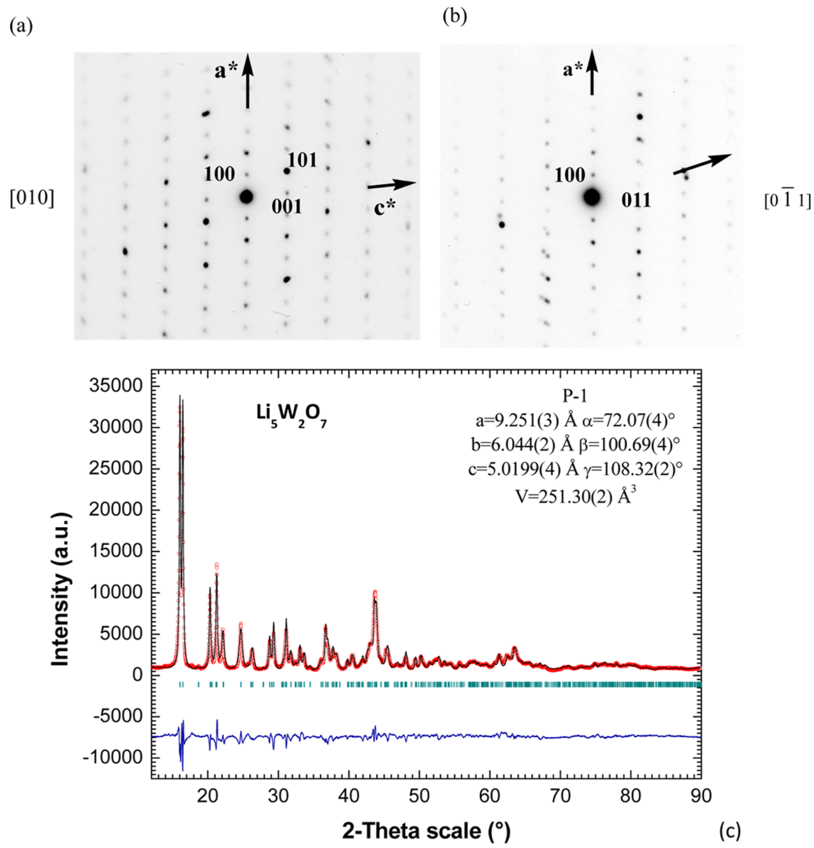

Figure 3. ED patterns recorded at room temperature along (a) [010] and (b) [0−11] and (c) Rietveld refinement plot of $Li_5W_2O_7$: observed X-ray diffraction intensity (○); calculated curve (line). The bottom curve is the difference of the patterns, $y_{obs} - y_{cal}$, and the small bars indicate the angular positions of the allowed Bragg reflections.

collected on a D8 diffractometer with Cu $K\alpha_1$ radiation. The ab initio structure calculation was carried out using the *FOX* program[16] and supposing that such a structure involves, like $Li_2W_2O_7$, only WO_6 octahedra. First, a pattern matching was performed with the *Fullprof*[17] program in order to refine the cell parameters, zero point, and shape of the peaks. The structural model was built up with two independent WO_6 octahedra, using the dynamical occupancy feature, implemented in *FOX*, to take into account oxygen atoms shared between the building blocks of octahedra. Before structure resolution, a Le Bail[18] fit was performed with the *FOX* program in order to find the best fit of the pattern. Because of the crystallite size effects in the pattern, resulting in a high overlapping of the peaks and, consequently a low quality of the data, the anti-bump and bond valence cost features were used with a scale factor of 500 for both. From the Rietveld refinements (Figure 3c), atomic coordinates were obtained (Table 2), which allow a structural model to be proposed for the $[W_2O_7]_\infty$ framework. The latter is also supported by the ED patterns, whose spot intensities calculated from these refinements are very similar to the experimental ones (Figure 3a).

From the projection of the $[W_2O_7]_\infty$ framework along the [720] direction (Figure 4a), it can be seen that the quadruple rows of edge-sharing octahedra running along the *c* axis exhibit a geometry similar to that observed for the structure of $Li_2W_2O_7$ (Figure 4b).

This explains that the *c* parameter remains practically unchanged in both structures and shows that the lithium intercalation takes place through a topotactic mechanism. In contrast, the $[W_2O_7]_\infty$ octahedral ribbons are significantly shifted with respect to each other in a tridimensional way, resulting in a significant modification of the triclinic cell. It is quite remarkable that insertion of three Li^+ cations into the $Li_2W_2O_7$ structure leads to a decrease of the cell volume by almost 7% (Table 1). In fact, reconstruction of the anionic framework, from the oxygen positions, even if they are not accurate, shows practically oxygen close packing of the ABC type, forming octahedral sites that can be occupied by the lithium cations. Thus, using valence bond calculations, we can

Table 2. Atomic Coordinates of Tungsten and Oxygen Obtained from Structure Refinement and of Lithium Proposed from Bond Valence Sum Calculations in $Li_5W_2O_7$

atom	*x*/*a*	*y*/*b*	*z*/*c*
W1	0.13782(8)	0.66321(9)	0.05218(16)
W2	0.27963(8)	0.60182(10)	0.64024(18)
O1	0.1140(5)	−0.0126(9)	0.7597(19)
O2	0.4862(9)	0.7031(13)	0.468(2)
O3	0.2580(6)	0.4887(13)	0.2903(19)
O4	0.0949(8)	0.4878(15)	0.766(2)
O5	0.4230(7)	0.4259(14)	0.8751(17)
O6	0.6617(8)	0.2357(14)	0.065(2)
O7	0.8271(5)	0.1870(9)	0.6356(12)
Li1	0.981	0.734	0.589
Li2	0.541	0.439	0.759
Li3	0.300	0.124	0.698
Li4	0.554	0.937	0.756
Li5	0.157	0.194	0.047

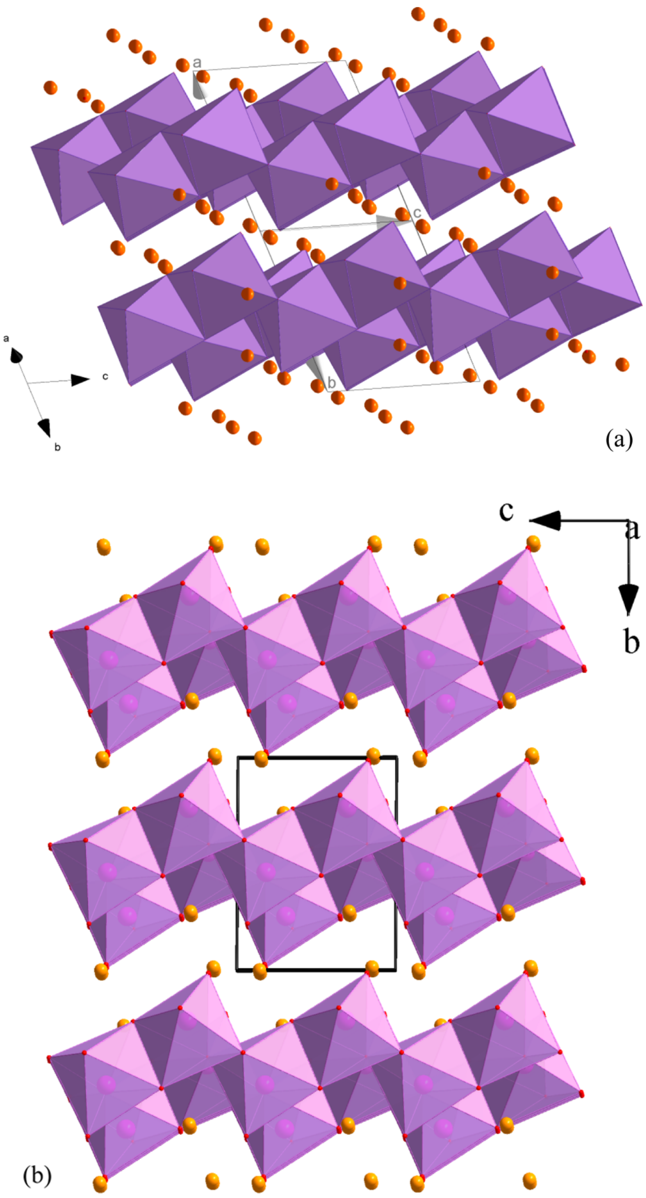

Figure 4. Comparison of the structural view along the [720] direction for $Li_5W_2O_7$ (a) and along the *a* axis for $Li_2W_2O_7$ (b). For clarity reasons, only the WO_6 octahedra are represented in order to emphasize the relationship between the ribbon-type structure $Li_2W_2O_7$ and reduced phase $Li_5W_2O_7$.

propose for the five Li^+ cations approximate positions (Table 2).

This leads for $Li_5W_2O_7$ to a distorted rock-salt-type structure (Figure 5), where the LiO_6 and WO_6 octahedra are displayed in an ordered way.

Because of the limited number of data, the W−O distances obtained from this PXRD study (Table 3) cannot be considered as accurate, and a combined neutron diffraction and X-ray synchrotron study will be necessary to establish this structure with accuracy and to confirm the positions of the Li^+ cations.

Electrochemical Behavior of $Li_{5-x}W_2O_7$. The charge−discharge profiles of this system have been performed by a galvanostatic cycling at C/10 in the potential window 1.3−3.0 V versus Li^+/Li (Figure 6).

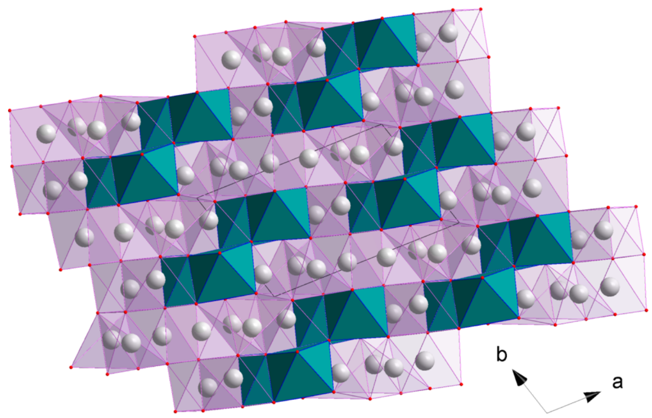

Figure 5. Representation of the $Li_5W_2O_7$ structure along the *c* axis, showing the rock-salt-type arrangement of the WO_6 and LiO_6 octahedra.

Table 3. Selected Distances W−O for $Li_5W_2O_7$

	distances/Å		distances/Å
W1−O3	1.8015	W2−O4	1.7849
W1−O6	1.9053	W2−O6	1.9261
W1−O4	1.9511	W2−O7	1.9283
W1−O7	1.9702	W2−O5	1.9531
W1−O1	2.1034	W2−O3	2.0289
W1−O4	2.2983	W2−O2	2.0799

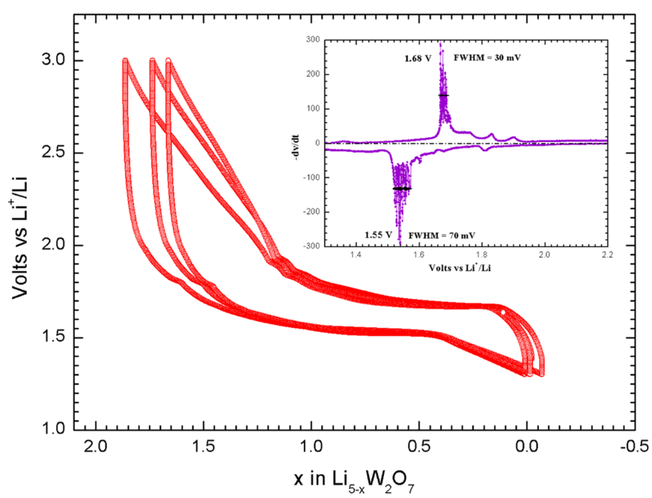

Figure 6. Potential versus capacity curve at C/10 in the 3.0−1.3 V potential window.

Starting from $Li_5W_2O_7$, a reversible capacity of two lithium molecules per formula unit (110 mAh/g) is obtained through a plateau at 1.68 V. As shown on the derivative curve (inset in Figure 6), the sharp redox peaks occur at 1.68 V upon charge and at 1.55 V upon discharge with a half-width length of 40 mV. The potentiodynamic titration curve (PITT, Figure 7) reveals a bell-shape-type response on the reversible phenomena and confirms, together with the sharpness of the peaks in the derivative curve, that the reversible process is biphasic.

Indeed, recording the chronoamperometric responses of the system during every potential level gives access to evolution of the kinetics with the redox level. This enables us to distinguish between a single-phase solid solution domain, in which the kinetics is governed by diffusion laws, and a two-phase domain,

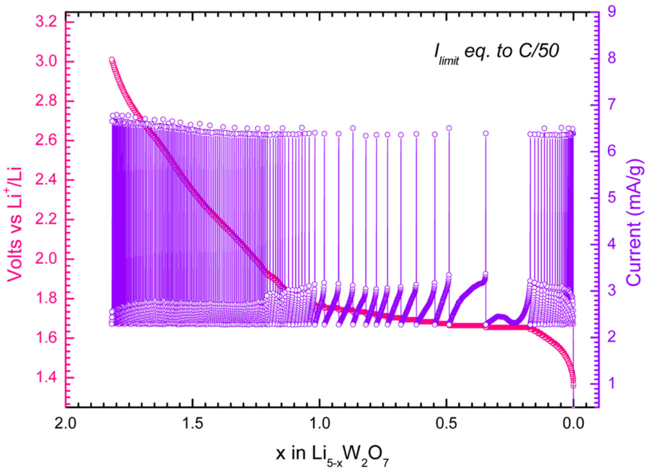

Figure 7. Potentiometric titration curve (PITT) during the first charge in the range of 3.0−1.3 V versus Li^+/Li with a limitation of the 10 mV potential step in a duration of 1 h and a current limitation equivalent to a galvanic current $I_{limit} = I_{C/50}$.

in which the kinetics is usually governed by the mobility of the interface between the two phases.[19−21] The plot of the discharge capacity versus cycle number (Figure 8) indicates a stable reversible capacity of 110 mAh/g even after 10 cycles for a C/10 rate.

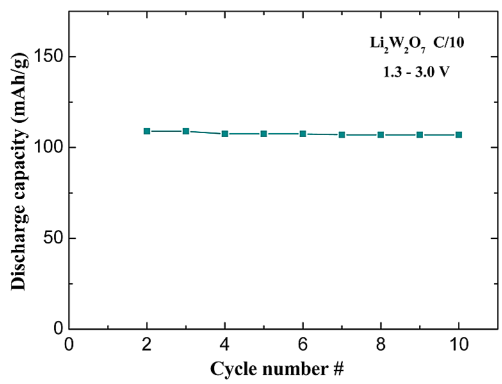

Figure 8. Specific discharge capacity versus cycle number. The potential window is 3−1.3 V, and the cycling rate is C/10.

Thus, the electrochemical process allows an intermediate oxidized phase $Li_3W_2O_7$ to be obtained, which can intercalate/deintercalate two lithium per formula unit reversibly. In contrast, all attempts to deintercalate more lithium from $Li_3W_2O_7$ were unsuccessful. In order to understand the nature of the intermediate oxidized phase, a chemical oxidation of $Li_5W_2O_7$ by NO_2BF_4 (2.1 V vs ENH) was carried out. An excess (5 times) of this strong oxidizing agent was added to the reduced oxide in acetonitrile and stirred for 5 days at room temperature. The atomic absorption analysis of the resulting product shows a composition close to $Li_{3.2\pm0.1}W_2O_7$, in agreement with the electrochemical cycling. The PXRD pattern of $Li_{3.2\pm0.1}W_2O_7$ (Figure 2c) shows that the structure of this phase seems to be related to that of $Li_5W_2O_7$ (Figure 2b) but is, nevertheless, too poorly crystallized to be investigated.

In summary, starting from the ribbon structure $Li_2W_2O_7$, the reduced phase $Li_{5-x}W_2O_7$ can be synthesized and can deintercalate/intercalate reversibly up to two lithium molecules per formula unit.

Mobility of Lithium in $Li_2W_2O_7$. The ribbon-type structure of the parent phase $Li_2W_2O_7$ and its ability to intercalate lithium suggest a good lithium mobility. Curiously, the ionic conductivity of $Li_2W_2O_7$ has never been explored to date to our knowledge. The impedance plots registered between 0.1 and 100 kHz for different temperatures (Figure 9a) show that this oxide is a cationic conductor because a semicircle is observed at high frequency, followed by a spike in the low-frequency region.

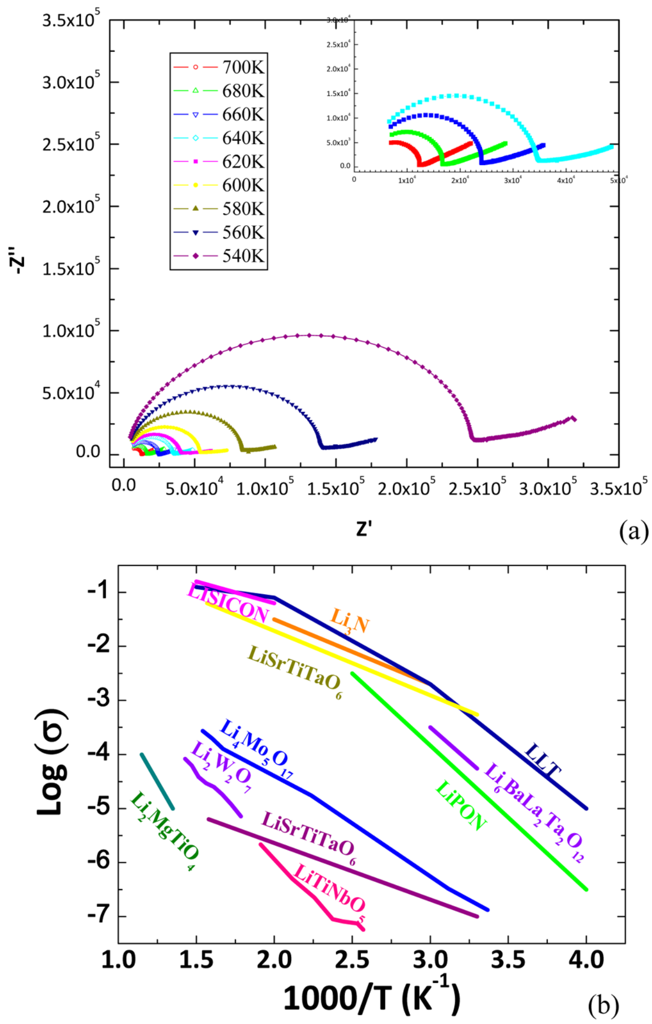

Figure 9. (a) Nyquist plots at various temperatures for $Li_2W_2O_7$. (b) Arrhenius plots of the lithium-ion conductivities (bulk) of selected metal oxides.

The ionic conductivity increases with the temperature, reaching ∼4 × 10^{-4} S/cm at 400 °C. The plot of log(σ) versus 1000/T (Figure 9b) shows a linear feature, obeying the classical Arrhenius relationship $\ln(\sigma T) = \ln(\sigma_0) - E_a/k_BT$. It evidences only one regime of conductivity characterized by an activation energy E_a = 0.5 eV. The conductivity is in the same range as other lithium-ion conductors[22] like the rock salts Li_2TiMgO_4[23] and $LiSrTiTaO_6$,[24] or the ribbon-type phase $Li_4Mo_5O_{17}$,[25] but also about 2 orders of magnitude less than the best candidates such as $Li_5La_3Nb_2O_{12}$, $Li_6BaLa_2Ta_2O_{12}$, Li_3N, or the phase $Li_{0.34}La_{0.51}TiO_2$ (LLT) (Table 4).[26−30] Unfortunately, the ionic conductivity of $Li_5W_2O_7$ could not be investigated because of its instability and rapid oxidation in air.

Table 4. Comparison of the Lithium-Ion Conductivity and Activation Energy Values for Lithium-Ion Conductors Reported in the Literature

formula	temperature range (K)	σ (S/cm)	E_a (eV)	ref
Li_3N	300–500	$10^{-2.7}$–$10^{-1.5}$		24
lipon $Li_{2.9}Si_{0.45}PO_{1.6}N_{1.3}$	250–400	$10^{-6.5}$–$10^{-2.5}$	0.45	24
lisicon $Li_{14}ZnGe_4O_{16}$	300–700	10^{-6}–$10^{-0.8}$	0.4–0.6	24, 27
$LiSrTiTaO_6$	300–640	$10^{-3.26}$–$10^{-1.2}$		21
$Li_6BaLa_2Ta_2O_{12}$	300–340	$10^{-4.26}$–$10^{-3.5}$	0.4–0.6	24
rock salt $Li_3Ni_3NbO_6$	300–600	10^{-3}–$10^{-1.5}$	0.37–0.45	27
rock salt Li_2MgTiO_4	700–900	10^{-4}–$10^{-2.5}$	0.53	23
lamellar $Na_{0.8}Co_{0.4}Ti_{0.6}O_2$	300–770	$10^{-5.23}$–$10^{-1.77}$	0.41	28
LLT $LaLi_{0.8}Ti_2O_6$	300–400	$10^{-3.3}$–$10^{-2.22}$	0.31	29
$Li_4Mo_5O_7$	300–700	$10^{-6.8}$–$10^{-3.4}$	0.35	25
$Li_2W_2O_7$	700	4×10^{-4}	0.5	this work

CONCLUSION

This study shows the great ability of the Li–W–O system to intercalate large amounts of lithium. It demonstrates that such a property is governed by the structural nature of the starting tungsten(VI) oxide, whose $[W_2O_7]_\infty$ ribbons exhibit, in fact, a rock-salt-type configuration and constitute an invariant during lithium intercalation, allowing topotactic extension toward the tridimensional rock-salt structure. This behavior is similar to that observed for the molybdate $Li_4Mo_5O_{17}$, whose $[Mo_5O_{17}]_\infty$ ribbons are an invariant, in lithium intercalation, allowing the rock-salt structure $Li_{12}Mo_5O_{17}$ to be generated.[22] However, it differs from the latter by the intercalation properties of the oxidized phase, which can deintercalate only two lithium molecules per formula unit. Thus, the research of lithium-rich transition-metal oxides appears as a promising route for the discovery of materials with intercalation properties. It must be emphasized that the lithium content that can be intercalated in those oxides will depend on the valence of the transition element and will require for the oxidized phase an oxidation state as high as possible. This suggests that, focusing on materials for applications in lithium-ion batteries, oxides with unusually high valence states of the transition element should be investigated in the future.

AUTHOR INFORMATION

Corresponding Author

*E-mail:valerie.pralong@ensicaen.fr. Tel: +33 2 31 45 26 32.

Author Contributions

All authors have given approval to the final version of the manuscript.

Notes

The authors declare no competing financial interest.

ACKNOWLEDGMENTS

The authors gratefully acknowledge the European Union (FEDER Originals Structures for Energy (OSE) Operation No. 33943), CNRS, the region Basse Normandie, and the Minister of Education and Research for financial support through their Research, Strategic, and Scholarship programs. G.V. thanks the CNRS and IFCPAR (Indo-French Centre for the Promotion of Advanced Research/Centre Franco–Indien Pour la Promotion de la Recherche Avancée) through Project 4608/2.

REFERENCES

(1) Ellis, B. L.; Lee, K. T.; Nazar, L. F. *Chem. Mater.* **2010**, *22*, 691–714.
(2) Poizot, P.; Laruelle, S.; Grugeon, S.; Dupont, L.; Tarascon, J.-M. *Nature* **2000**, *407*, 496–499.
(3) Armand, M.; Tarascon, J.-M. *Nature* **2008**, *451*, 652–652.
(4) Whittingham, M. S. *Chem. Rev.* **2004**, *104*, 4271–4301.
(5) Pralong, V. *Prog. Solid State Chem.* **2009**, *37* (4), 262–277.
(6) Gerand, B.; Nowogrocki, G.; Guenot, J.; Figlarz, M. *J. Solid State Chem.* **1979**, *29*, 429–434.
(7) Hernan, L.; Macias, M.; Morales, J.; Sanchez, L.; Tirado, J. L. *Solid State Ionics* **1991**, *48*, 231–240.
(8) Driouiche, A.; Figlarz, M.; Delmas, C. *Solid State Ionics* **1993**, *62*, 113–117.
(9) Morikawa, H.; Okada, K.; Marumo, F.; Iwai, S. I. *Acta Crystallogr., Sect. B* **1975**, *31*, 1451–1454.
(10) Magarill, S. A.; Klevtsova, R. F.; Bakakin, V. V. *Kristallografiya* **1973**, *18*, 269.
(11) Zachariasen, W. H.; Plettinger, H. A. *Acta Crystallogr.* **1961**, *14*, 229–230.
(12) Hoffmann, R.; Hoppe, R. *Z. Anorg. Allg. Chem.* **1989**, *573*, 157–169.
(13) Pralong, V.; Delahaye-Vidal, A.; Chabre, Y.; Tarascon, J. M. *J. Solid State Chem.* **2001**, *162*, 270–281. Pralong, V.; Chabre, Y.; Delahaye-Vidal, A.; Tarascon, J. M. *Solid State Ionics* **2002**, *147*, 73–84.
(14) Smith, G. S.; Snyder, R. L. *J. Appl. Crystallogr.* **1979**, *12*, 60–65.
(15) Favre-Nicolin, V.; Cerny, R. *J. Appl. Crystallogr.* **2002**, *35*, 734–743.
(16) Cerny, R.; Favre-Nicolin, V. *Powder Diffr.* **2005**, *20*, 359–365.
(17) Rodriguez-Carvajal, J. *Physica B* **1993**, *192*, 55–69.
(18) Le Bail, A.; Duroy, H.; Fourquet, J. L. *Mater. Res. Bul.* **1988**, *23*, 447–450.
(19) Thompson, A. H. *J. Electrochem. Soc.* **1979**, *126*, 603.
(20) Chabre, Y. *Physics of Intercalation II*; NATO ASI Series B305; Plenum Press: New York, 1993; p 181
(21) Shin, H. C.; Pyun, S. I. *Electrochim. Acta* **1999**, *44*, 2235–2244.
(22) Knauth, P. *Solid State Ionics* **2009**, *180*, 911–916.
(23) Kishore, M. S.; Marinel, S.; Pralong, V.; Caignaert, V.; D'Astorg, S.; Raveau, B. *Mater. Res. Bull.* **2006**, *41*, 1378–1384.
(24) Thangadurai, V.; Weppner, W. *Ionics* **2002**, *8*, 281–292.
(25) Pop, N.; Pralong, V.; Caignaert, V.; Colin, J. F.; Malo, S.; Van Tendeloo, G.; Raveau, B. *Chem. Mater.* **2009**, *21*, 3242–3250.
(26) Thangadurai, V.; Weppner, W. *Ionics* **2006**, *12*, 81–92.
(27) Sebastian, L.; Gopalakrishnan, J. *J. Mater. Chem.* **2003**, *13*, 433–441.
(28) Thangadurai, V.; Adams, S.; Weppner, W. *Chem. Mater.* **2004**, *16*, 2998–3006.
(29) Bruce, P. J.; West, A. R. *J. Electrochem. Soc.* **1983**, *130*, 662–669.
(30) Shin, Y.-J.; Park, M.-H.; Kwak, J.-H.; Namgoong, H.; Hee Han, O. *Solid State Ionics* **2002**, *150*, 363–372.